

## THIN-LAYER CELL ELECTRODEPOSITION: STABLE AND UNSTABLE FLOWS

G. Marshall\*, E. Mocskos\*, G. Gonzalez\*, S. Dengra\* and F. V. Molina†

\*Laboratory for Complex Systems, Computer Science Department,  
Faculty of Exact and Natural Sciences,  
University of Buenos Aires, (1428) Buenos Aires, Argentina  
e-mail: marshalg@mail.retina.ar, emocskos@dc.uba.ar,  
ggonzale@dc.uba.ar, sdengra@dc.uba.ar  
web page: <http://www.dc.uba.ar/people/proyinv/fra/>

†INQUIMAE, Faculty of Exact and Natural Sciences,  
University of Buenos Aires, (1428) Buenos Aires, Argentina  
e-mail: fmolina@qi.fcen.uba.ar

**Key Words:** Electrodeposition, computational modeling, finite differences, stable physico-chemical hydrodynamic flows, unstable physicochemical hydrodynamic flows.

**Abstract.** *Electrodeposition in thin cells of different orientations relative to gravity leads to complex stable and unstable physicochemical hydrodynamic flows. Here we present a theoretical macroscopic 3D model and numerical simulations describing such flows. The model consists in the Nernst-Planck equations for ion transport, the Poisson equation for the electric field and the Navier-Stokes equations for the fluid flow. These equations are solved in a uniform grid using finite differences and a strongly implicit iterative scheme. Our model predicts that when the cathode is above the anode the flow becomes stable as long as there is no growth. When growth is present, the model predicts zones of lowered concentration, adjacent to a downwards growing finger, inducing a gravity driven convective vortex roll wrapped to the finger. In a vertical cell with the anode above the cathode, the model predicts the existence of an unstable flow in the form of plumes emanating from each cathode, expanding toward one another and mixing. For both cases, in the presence of growth, the model predicts the existence of an electrically driven vortex ring at the dendrite tip; it allows fluid to penetrate the dendrite tip and to be ejected from its side. Such behavior has been observed in experiments.*

## 1 INTRODUCTION

In an ECD experiment, the electrolytic cell consists of two glass plates sandwiching two parallel electrodes and a metal salt electrolyte. A voltage difference applied between electrodes produces a ramified deposit by reduction of the metal ions. Depending in the cell geometry, electrolyte concentration, cell voltage and other parameters, the deposit can be fractal, densely branched or dendritic.<sup>1-22</sup>

Dendrite growth induces a complex physicochemical hydrodynamical ion transport process. Ion transport is mainly governed by diffusion, migration and convection. Convection is mostly driven by coulombic forces due to local electric charges and by buoyancy forces due to concentration gradients that lead to density gradients.

Convection adds to the complexity of ECD flows and therefore it is natural to try to reduce it to a negligible level. One possibility is to reduce buoyancy forces orienting the cell in a vertical position in relation to gravity.<sup>12</sup> Here we follow this alternative. With this technique, when the cathode (and low density fluid) is above the anode (and high density fluid), the invasion of the cell by the gravity induced rolls is globally suppressed<sup>12</sup> while electroconvection remains. However, if the anode (and high density fluid) is above the cathode (and low density fluid) an unstable stratification leads to a global convective flow.<sup>12</sup>

## 2 THE PHYSICS AND MATEMATICS OF ECD FLOWS IN A VERTICAL POSITION

In this section we describe the experimental measurements carried out in ECD experiments in a vertical cell in the stable and unstable regimes, and the phenomenological and mathematical models describing it.

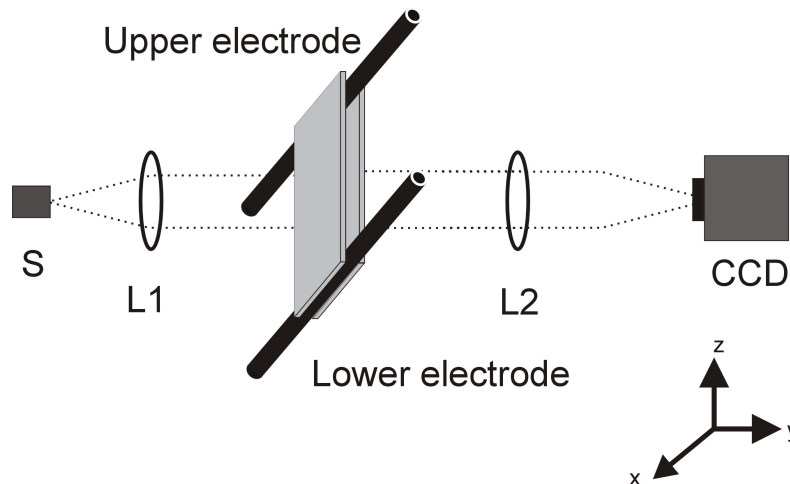


Figure 1: Experimental setup

Figure 1 shows a typical cell in a vertical position used in ECD experiments. Here, the vertical plane or  $zx$  plane contains the electrodes and the growing dendrites (the cathode-anode distance is measured along the  $z$  coordinates).

We now present the phenomenological model. In an ECD experiment in a vertical cell (with the cathode above the anode), when the circuit is closed, current starts flowing through the cell and ion concentration boundary layers develop near each electrode. At the anode the concentration is increased above its initial level due to the transport of anions towards, and the dissolution of metal ions from the anode. At the cathode, the ion concentration is decreased as metal ions are reduced and deposited out and anions drift away. These concentration variations lead to density variations, and therefore to concentration fronts at the electrodes. In this configuration the high density fluid is below the low density fluid, hence a stable stratified flow emerges in which gravitoconvection is suppressed. Stratification remains stable as long as there is no growth. This constitutes a fully stable situation in which there is no convection and ion transport is mainly diffusive and migratory: the cathodic and anodic concentration fronts being lighter and heavier, respectively, than the fluid adjacent, do not detach from their respective electrodes. During this initial period, cation depletion at the cathode is supposed uniform. Simultaneously, in a very narrow region near the cathode a local charge develops, giving rise to local electric forces initially pointing towards the cathode (hence no electroconvection arises).

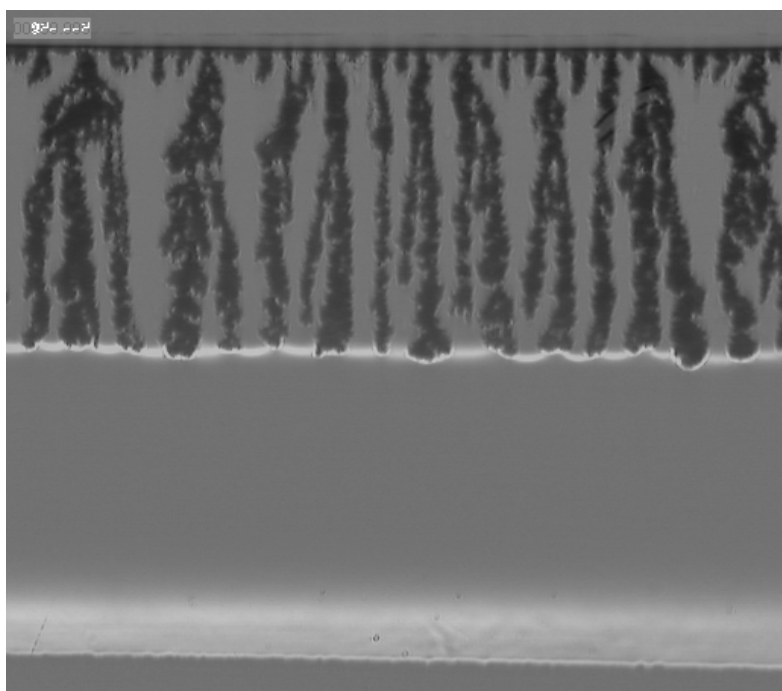


Figure 2: Stable flow pattern: a schlieren image of vertical oriented cell at 460s. Copper sulfate solution concentration is 0.1M, the cell dimensions are  $70 \times 10 \times 0.2 \text{ mm}^3$  and the applied constant current is 5mA.

After a few seconds, an instability develops, triggering the growth of a deposit at the cathode. The deposit develops as a three-dimensional (3D) array of thin porous metallic filaments. Electric forces concentrate at the tips; each porous filament allows fluid to penetrate its tip and to be ejected from the sides, forming a vortex ring driven by the electric force. Figure 2 shows a schlieren snapshot of the deposit front (dark pixels) and the cathodic and anodic concentra-

tion fronts (light pixels) when 460 s have elapsed from the beginning of the experiment. The deposit front looks rather smooth in the average, dendrite tips surrounded by tenuous concentration arches joining neighboring tips. The shape of the arches is the result of electroconvection (previously discussed) and gravitoconvection (later explained).

Stratification breaks down as soon as growth appears. This is because the fluid concentration surrounding a downward growing dendrite tip diminishes, creating an horizontal concentration gradient and thus, locally gravitoconvection. This local instability is analyzed next.

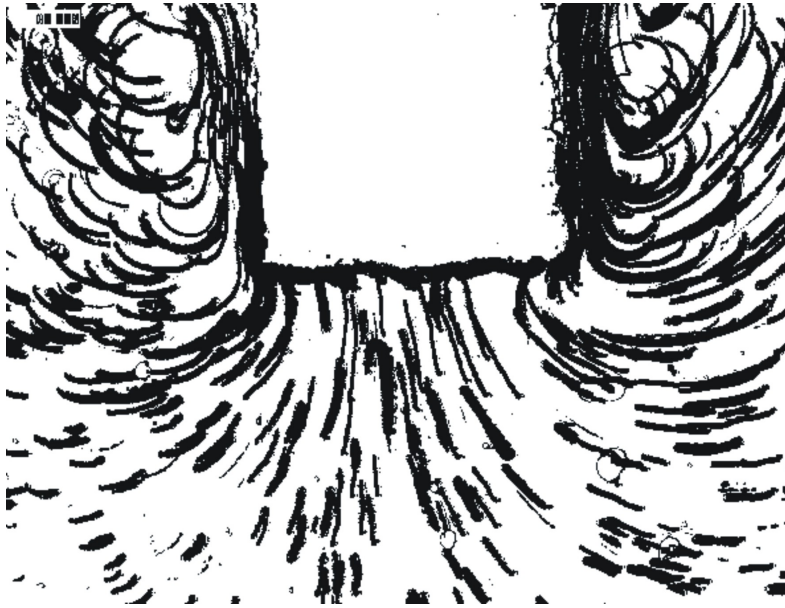


Figure 3: Stable flow pattern: visualization of  $1\mu\text{m}$  sized particle trajectories near the cathode. To show the motion of tracer particles 200 digital images were superimposed: from 0 to 20s. Copper sulfate solution concentration is 0.1M with 30% glycerol in weight, the cell dimensions are  $70 \times 10 \times 0.127\text{ mm}^3$ , the applied constant current is 2mA and the spike dimensions are  $1 \times 0.5 \times 0.127\text{ mm}^3$

Figure 3 shows an ECD experiment in a vertical cell with a flat cathode with a small protruding spike (to mimic the behavior of one of the dendrite tips) and the flow surrounding it. Convection is visualized with 200 snapshots of micron sized tracer particles, spanning an interval of 20 s, superposed to show their motion. They appear as a pair of counter-rotating vortices, the result of the vector composition of local buoyancy and local electric forces. In this stable regime there is local convection, but globally the ECD process is migration and diffusion controlled.

In an ECD experiment in a vertical cell (with the anode above the cathode), when the circuit is closed, current starts flowing through the cell and ion concentration boundary layers develop near each electrode as in the stable case, leading to convection rolls at the electrodes. However, in this configuration the high density fluid is above the low density fluid and instability is inevitable. This is illustrated in figure 4 showing a schlieren snapshot of the concentration.

The genesis of this unstable flow is the following. In the first stages, before growth starts,

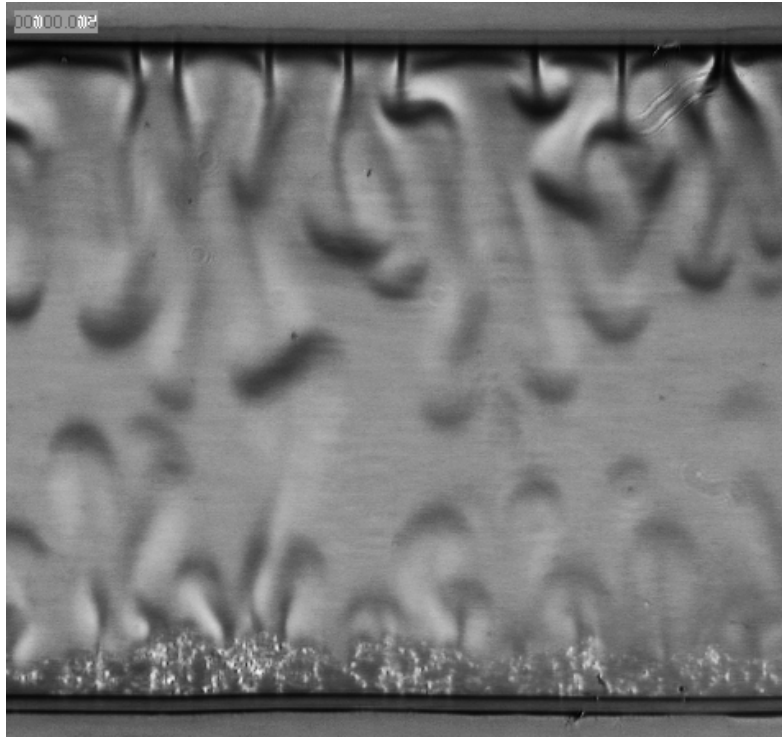


Figure 4: Unstable flow pattern: schlieren image of a vertically oriented cell at 100s. Copper sulfate solution concentration is 0.1M, the cell dimensions are  $70 \times 10 \times 0.2 \text{ mm}^3$  and the applied constant current is 5mA.

the cathodic and anodic concentration fronts being heavier and lighter, respectively, than the fluid adjacent, tend to detach from their respective electrodes. Simultaneously, as in the stable case, local charges develop near the cathode giving rise to local electric forces initially pointing towards the cathode.

Instants later, as in the stable case, an instability develops, triggering the growth of a deposit at the cathode in the form of a three-dimensional (3D) array of thin porous metallic filaments. Electric forces concentrate at their tips driven fluid in the form of vortex rings. In relation to electric forces, the situation is completely analogous to the stable case, the electric field being invariant relative to variations in the cell position. Figure 4 shows that, as time evolves, the instability develops leading to a global gravitoconvective flow consisting in high density plumes descending from the anode and low density plumes rising from the cathode. This global gravitoconvection strongly inhibits dendrite growth.

We now present the mathematical model. Ion transport in thin-layer ECD can be described with a mathematical model based on first principles,<sup>23-26</sup> including the Nernst-Planck equations for ion transport, the Poisson equation for the electric potential, and the Navier-Stokes equations for the fluid flow. The 3D dimensionless system of equations can be written as

$$\frac{\partial C_i}{\partial t} = -\nabla \cdot \mathbf{j}_i \quad (1)$$

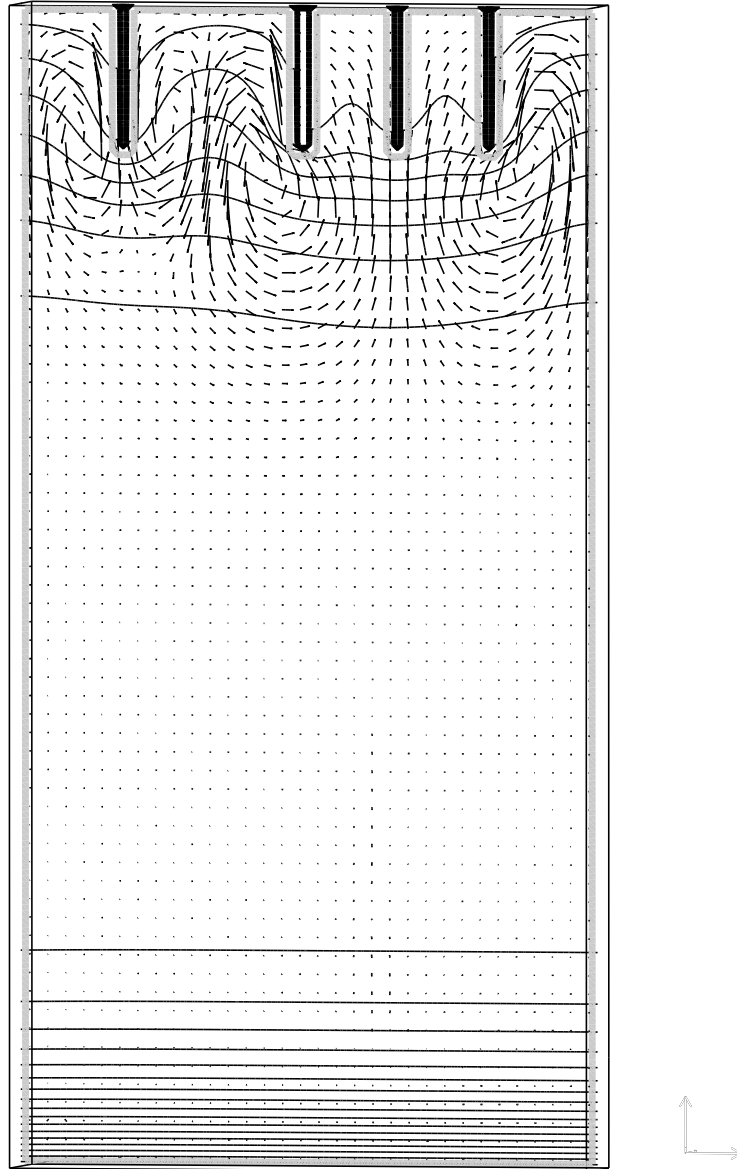


Figure 5: Global stable flow pattern simulation: velocity field superimposed with anion concentration isocontour lines.

$$\mathbf{j}_i = -M_i C_i \nabla \phi - \frac{1}{Pe_i} \nabla C_i + C_i \mathbf{v} \quad (2)$$

$$\nabla^2\phi = Po \sum_i z_i C_i \quad (3)$$

$$\frac{\partial \zeta}{\partial t} + \nabla \times (\zeta \times \mathbf{v}) = \frac{1}{Re} \nabla^2 \zeta + \sum_i \left[ G_{e_i} z_i (\nabla \phi \times \nabla C_i) - G_{g_i} (\nabla \times C_i) \cdot \frac{\mathbf{g}}{g} \right] \quad (4)$$

$$\zeta = -\nabla^2 \Psi \quad (5)$$

$$\mathbf{v} = \nabla \times \Psi \quad (6)$$

Here  $C_i$  and  $\mathbf{j}_i$  are the dimensionless concentration and flux of an ionic species  $i$  (for a ternary electrolyte such as  $\text{ZnSO}_4/\text{H}_2\text{SO}_4$ ,  $i = \text{C, A and H}$ , standing for zinc, sulphate and hydrogen ions);  $\mathbf{v}$ ,  $\phi$ ,  $\zeta$  and  $\Psi$  are the dimensionless fluid velocity, electrostatic potential, vorticity vector and velocity potential vector, respectively;  $\mathbf{g}/g$  is a unit vector pointing in the direction of gravity. The quantities  $M_i = \mu_i \Phi_0 / x_0 u_0$ ,  $Pe_i = x_0 u_0 / D_i$ ,  $Po = x_0^2 C_0 e / \epsilon \Phi_0$ ,  $Re = x_0 u_0 / \nu$ ,  $G_{e_i} = e C_i \Phi_0 / \rho_0 u_0^2$  and  $G_{g_i} = x_0 C_i g \alpha_i / u_0^2$ , stand for the dimensionless numbers Migration, Peclet, Electric Poisson, Reynolds, Electric Grashof and Gravity Grashof numbers, respectively. The quantities  $z_i$ ,  $\mu_i$ , and  $D_i$  are, respectively, the number of charges per ion, mobility and diffusion constants of an ionic species  $i$ ;  $\mu_i$  and  $z_i$  are signed quantities, being positive for cations and negative for anions;  $g$  is the dimensional gravitational acceleration;  $e$  is the electronic charge,  $\epsilon$  is the permittivity of the medium and  $\nu$  is the kinematic viscosity.  $x_0$ ,  $u_0$ ,  $\phi_0$ ,  $C_0$ , and  $\rho_0$  are reference values of the length, velocity, electrostatic potential, concentration, and fluid density, respectively. For system closure, a Boussinesq-like approximation has been used for the fluid density:  $\rho = \rho_0 (1 + \sum_i \alpha_i \Delta C_i)$ , where  $\alpha_i = \frac{1}{\rho_0} \frac{\partial \rho}{\partial C_i}$ .

System (1-6), with appropriate initial and boundary conditions, is valid in a space-time domain defined by  $\mathbf{G} = [\Omega(\mathbf{t})\mathbf{x}(\mathbf{0}, \mathbf{t})]$ , where  $\Omega$  is a three-dimensional region with boundary  $\Gamma(t)$ ; this boundary moves with speed proportional to the norm of the flux  $\mathbf{j}_i$ . The boundary conditions for the velocity potential vector are discussed, for instance, in Mallinson et al.<sup>27</sup> in a plane impermeable surface, the vector is normal to the surface and its gradient is zero; at nonslip surfaces, the tangential derivative of the velocity components are zero.

### 3 NUMERICAL RESULTS

In the following we show numerical simulations of ECD experiments with the cell in a vertical position in the stable and unstable modes. The stable mode, i.e., when the cathode is above the anode, is shown first.

The cell is represented by a cubic grid of  $100 \times 200 \times 10$  nodes. The dimensionless numbers used are:  $M_a = 1/30$ ,  $M_c = 1/45$ ,  $Pe_a = 600$ ,  $Pe_c = 750$ ,  $Po = 4.42 \times 10^{-3}$ ,  $Re = 0.1$ ,  $Ge = 1 \times 10^{-3}$ ,  $Gg_a = 1.5 \times 10^5$  and  $Gg_c = 1.0 \times 10^5$ .

Figure 5 presents the simulation of a stable case in which dendrites are represented by four spikes or fingers of equal length. This configuration mimics the situation depicted in figure 2.

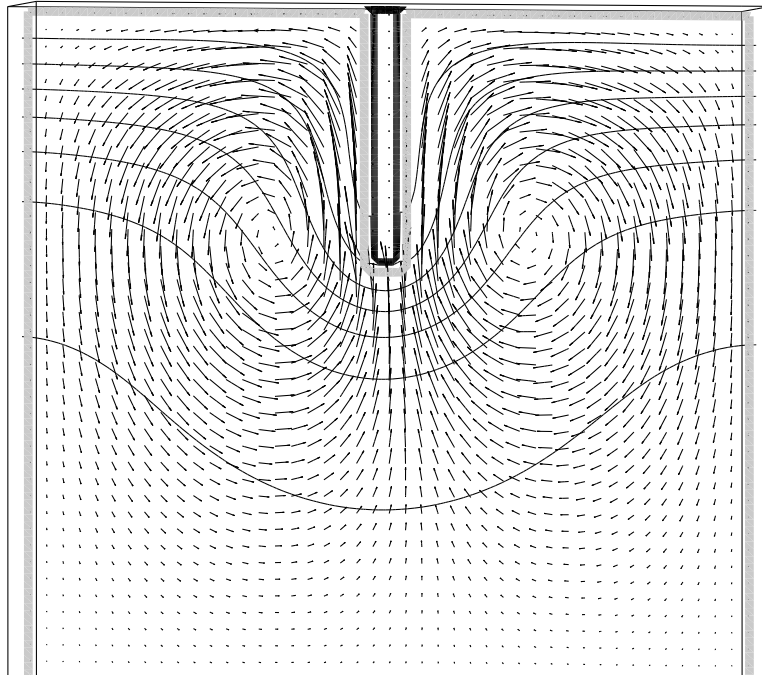


Figure 6: Stable flow pattern simulation near a spike (enlarged): velocity field superimposed with anion concentration isocontour lines.

In the figure, the contour lines of the concentration at the finger tips (in a longitudinal cross-section at the center of the cell) are slightly curved at the spike front as in the experiments. The arch joining two neighboring fingers separate two zones: the inner zone of the arch is depleted of ions while the outer zone rapidly reaches the bulk concentration value, as observed in the experiments.<sup>28</sup>

Figure 6 shows a simulation of the pattern flow near a spike in a stable flow in a longitudinal cross-section at the cell center. The figure reveals the existence of a pair of vortices surrounding the tip. They are the result of the composition of the electric and gravity vortex rings.

Figure 7 presents the simulation of an unstable case in which dendrites are represented just by one small spike at the cathode center. This configuration intents to mimic the situation depicted in figure 4. The figure shows a snapshot of a fully developed unstable flow revealing the high density plumes descending and mixing with ascending low density ones.

#### 4 CONCLUSIONS

We introduced a 3D theoretical macroscopic model for ECD in cells in a vertical position in the stable and unstable cases, and preliminary numerical simulations. Our model predicts that in the stable case (cathode above anode) when growth is present the fluid concentration near a downward growing tip is lowered thus generating a vortex tube (driven by gravitoconvection) superposed to a vortex ring (driven by electroconvection) wrapping the dendrite tip (much as in the case of the horizontal cell in which the dendrite tip is surrounded by gravito- and electro-

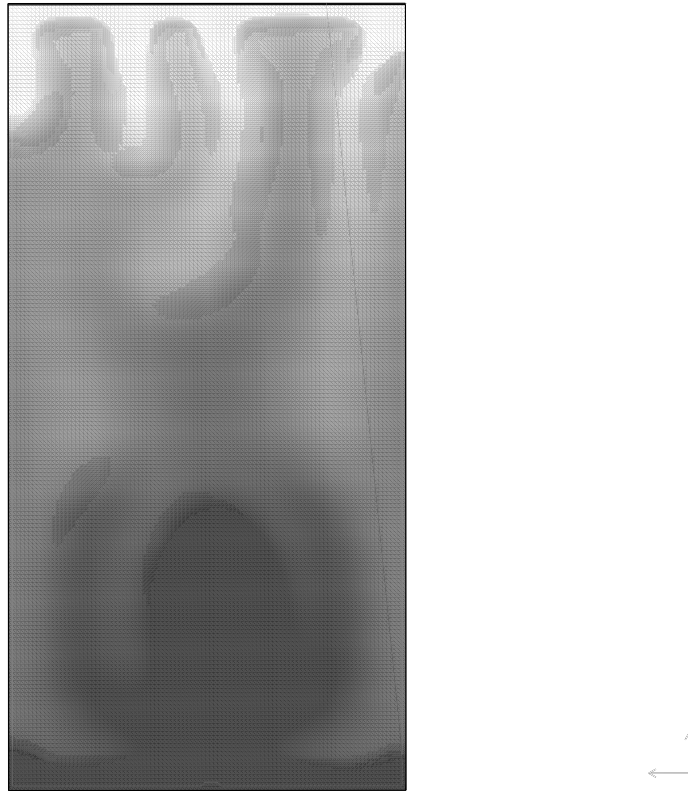


Figure 7: Inestable flow pattern simulation: anion concentration.

convective vortices, respectively) . The region close to the anode is not affected by the growth and remains without convection.

In the unstable case, our model predicts that the cathodic and anodic vortex tubes transform themselves into plumes or tongues expanding towards one another and merging. As a consequence of this mixing concentration gradients are strongly attenuated. In the stable as well as in the unstable cases, our model predicts that in the presence of growth, a vortex ring driven by electroconvection exists at the tips of the dendrites, allowing fluid to penetrate at the tip and be ejected from its sides. Flow at the tips is the result of vortex tube and vortex ring superposition: both have the same sign, that is, at the tip's left and right sides, both vortices are clockwise and counter clockwise, respectively.

**ACKNOWLEDGEMENTS:**G. M. and F. V. M. are investigators of the CONICET, Argentina. This work is partially supported by UBACYT grant No. X187/2001, ANPCyT grant No. PICTR 184, and CONICET grant No. PIP379/98.

## REFERENCES

- [1] T. Vicsek. *Fractal Growth Phenomena*. World Scientific, Singapore, 2nd edition, (1992).

- [2] F. Argoul, J. Huth, P. Merzeau, A. Arneodo and H. L. Swinney. Experimental evidence for homoclinic chaos in an electrochemical growth process. *Physica D*, **62**(170) (1993).
- [3] R. M. Brady and R. C. Ball. Fractal growth of copper electrodeposits. *Nature*, **309**, 225 (1984).
- [4] V. Fleury, J. N. Chazalviel, M. Rosso, and B. Sapoval. Experimental Aspects of Electrochemical Deposition of Copper Aggregates. *Phys. Rev. A*, **44**, 6693 (1991).
- [5] V. Fleury, J. N. Chazalviel and M. Rosso. Theory and Experimental Evidence of Electroconvection around Electrochemical Deposits. *Phys. Rev. Lett.*, **68**, 2492 (1992).
- [6] V. Fleury, J. N. Chazalviel and M. Rosso. Coupling of Diffusion, Migration and Convection in the Vicinity of Electrochemical Deposits. *Phys. Rev. E*, **48**, 1279 (1993).
- [7] V. Fleury, J. Kaufman and B. Hibbert. A Mechanism of Morphology Transition in Ramified Electrodeposition. *Nature*, **367**, 435 (1994).
- [8] K. A. Linehan and J. R. de Bruyn. A Mechanism of Morphology Transition in Ramified Electrodeposition. *Can. J. Phys.*, **73**, 177 (1995).
- [9] V. Fleury, M. Rosso, and J. N. Chazalviel. Electrochemical Deposition Without Supporting Electrolyte. In B. Sapoval F. Family, P. Meakin and R. Wool, editors, *MRS Symposia Proc*, Boston, (1994). Material Research Society.
- [10] V. Fleury, M. Rosso and J. N. Chazalviel. Diffusion Migration and Convection in Electrochemical Deposition, Vortex Pairs, Vortex Rings Arches and Domes. In H.D. Merchant, editor, *symposium on "Structure and Properties of Deposits"*, pages 195–217, Warrendale penn, (1995). 3M (Metals Minerals and Materials Society), TMS Publications.
- [11] V. Fleury and J.N. Chazalviel. 2-D and 3-D Convection During Electrochemical Deposition, Experiments and Models. In B. Sapoval F. Family, P. Meakin and R. Wool, editors, *MRS Symposia Proc*, Boston, (1994). Material Research Society.
- [12] J. Huth, H. Swinney, W. McCormick, A. Kuhn and F. Argoul. Role of convection in thin-layer electrodeposition. *Phys. Rev. E*, **51**, 3444 (1995).
- [13] D. Barkey, D. Watt, Z. Liu, and S. Raber. The role of induced convection in branched electrodeposit morphology selection. *J. Electrochem. Soc.*, **141**(5), 1206 (1994).
- [14] C. Leger, J. Elezgaray, and F. Argoul. Experimental demonstration of diffusion-limited dynamics in electrodeposition. *Phys. Rev. Lett.*, **78**, 5010 – 5013 (June 1997).
- [15] J. N. Chazalviel. Electrochemical aspects of the generation of ramified metallic electrodeposits. *Phys. Rev. A*, **42**, 7355–7367 (December 1990).
- [16] G. Marshall, E. Perone, P. Tarela and P. Mocskos. A macroscopic model for growth pattern formation of ramified copper electrodeposits. *Chaos, Solitons and Fractals*, **6**, 315 (1995).
- [17] G. Marshall and P. Mocskos. Growth model for ramified electrochemical deposition in the presence of diffusion, migration, and electroconvection. *Phys. Rev. E*, **55**, 549–563 (January 1997).
- [18] G. Marshall, P. Mocskos, H. L. Swinney and J. M. Huth. Buoyancy and electrically driven convection models in thin-layer electrodeposition. *Phys. Rev. E*, **59**, 2157–2167 (February 1999).
- [19] S. Dengra, G. Marshall and F. Molina. Growth model for ramified electrochemical depo-

- sition in the presence of diffusion, migration, and electroconvection. *J. Phys. Soc. Japan*, **69**, 963–971 (March 2000).
- [20] G. Gonzalez, G. Marshall, F. V. Molina, S. Dengra and M. Rosso. Viscosity effects in thin-layer electrodeposition. *J. Electrochem. Soc.*, **148**(7), C479–C487 (July 2001).
- [21] G. Gonzalez, G. Marshall, F. V. Molina and S. Dengra. Transition from gravito- to electroconvective regimes in thin-layer electrodeposition. *Phys. Rev. E*, **65**(5), 051607 (May 2002).
- [22] G. Marshall, E. Mocskos, F. V. Molina, and S. Dengra. Three-dimensional nature of ion transport in thin-layer electrodeposition. *Phys. Rev. E*, **68**(2), 021607 (August 2003).
- [23] A. J. Bard and L. R. Faulkner. *Electrochemical Methods, Fundamentals and Applications*. Wiley, New York, (1980).
- [24] J. S. Newman. *Electrochemical Systems*. Prentice Hall, New Jersey, (1973).
- [25] Ronald F. Probstein. *Physicochemical Hydrodynamics, An Introduction*. Wiley, New York, (1994).
- [26] V. G. Levich. *Physicochemical Hydrodynamics*. Prentice Hall, New Jersey, (1962).
- [27] G. D. Mallinson and G. de Vahl Davis. Three-dimensional natural convection in a box: A numerical study. *Journal of Fluid Mechanics*, **83**(1) (1977).
- [28] S. Dengra. *Estudios experimentales y teóricos del transporte iónico en electrodeposición en celdas delgadas*. PhD thesis, Computer Science Department, Buenos Aires University, (August 2004).